Supporting information

Construction of parallel-structured composites based on theoretical model to achieve ultra-high dielectric constant

Ruolin Han[a], Jiafei Ren[a], Hui Quan[b], Xuehe Wang[a], Wenning Qi[a], Dali Gao[b,*], Zheng Zhou[a], Qifang Li[a], Guang-Xin Chen[a,*]

[a] *College of Material Science and Engineering, Beijing University of Chemical Technology, Beijing, 100029 PR China*

[b] *Sinopec Beijing Research Institute of Chemical Industry, Beijing, 100013, PR China*

Corresponding Authors

*E-mail: gaodl.bjhy@sinopec.com. (Dali Gao).

*E-mail: gxchen@mail.buct.edu.cn. (Guang-xin Chen).

Theoretical models[1, 2] for predicting effective dielectric constant of composites.

Lichtenecker model: $\varepsilon^k = V_1 \varepsilon_1^k + V_2 \varepsilon_2^k$ eq.S1

Parallel model: $\varepsilon = V_1 \varepsilon_1 + V_2 \varepsilon_2$ eq.S2

Series model: $\varepsilon = \dfrac{\varepsilon_1 \varepsilon_2}{V_1 \varepsilon_1 + V_2 \varepsilon_2}$ eq.S3

Maxwell-Garnett model: $\varepsilon = \varepsilon_2 \dfrac{(2V_1 + 1)V_2 + 2(1 - V_1)\varepsilon_2}{(1 - V_1)\varepsilon_1 + (2 + V_1)\varepsilon_2}$ eq.S4

Jayasundere-Smith model: $\varepsilon = \dfrac{V_2 \varepsilon_2 + V_1 \varepsilon_1 \dfrac{3\varepsilon_2}{\varepsilon_1 + \varepsilon_2}\left[1 + \dfrac{3V_1(\varepsilon_1 - \varepsilon_2)}{\varepsilon_1 + \varepsilon_2}\right]}{V_2 + V_1 \dfrac{3\varepsilon_2}{\varepsilon_1 + \varepsilon_2}\left[1 + \dfrac{3V_1(\varepsilon_1 - \varepsilon_2)}{\varepsilon_1 + \varepsilon_2}\right]}$ eq.S5

Where ε is the dielectric constant of the composites. V_1 and V_2 are the volume fractions of fillers and polymer matrixes, respectively. ε_1 and ε_2 are the dielectric constants of fillers and polymer matrixes, respectively.
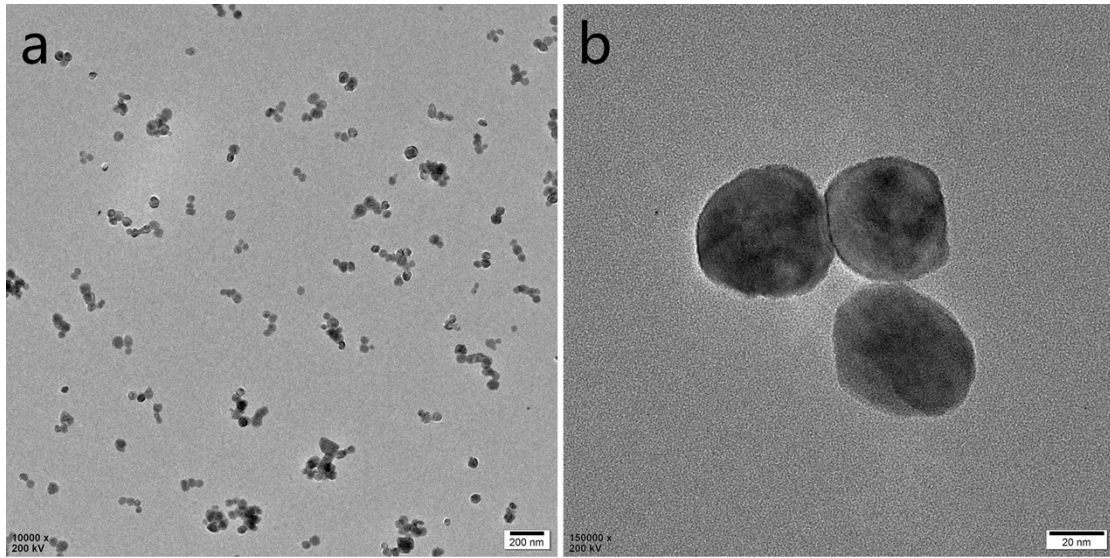
Figure S1. TEM images of the BT particles.

In this work, the diameter of the BT particles used to prepare the BT/EP composites was about 50 nm.
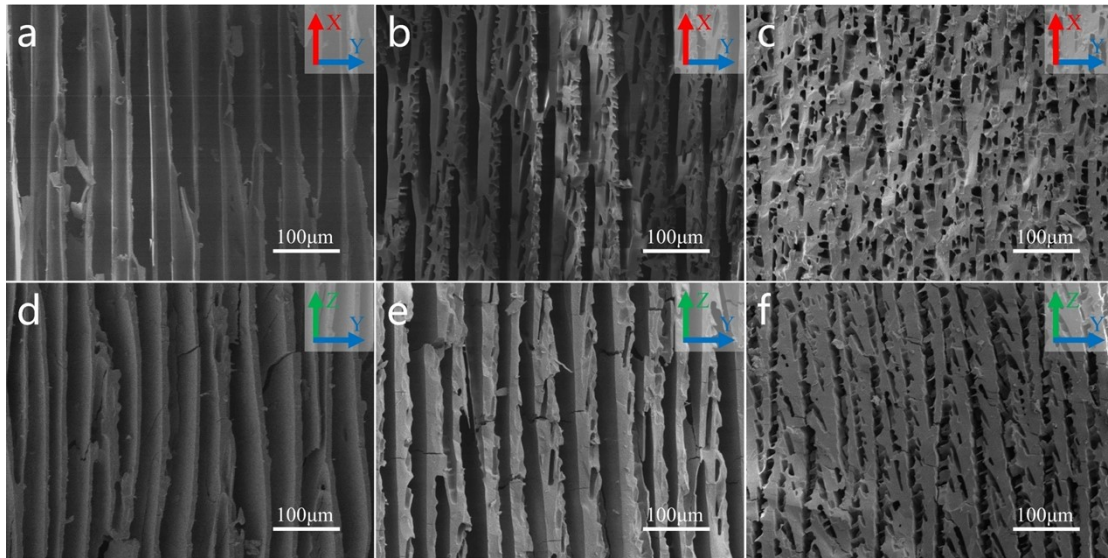
Figure S2. SEM images of the BT skeletons before sintering viewed along the (a, b, c) Z-axis and along the (d, e, f) X-axis. These skeletons were prepared from BT suspensions with (a, d) 10, (b, e) 20 and (c, f) 30 vol.% solid content.

The BT skeletons containing organic components such as PVA were prepared by bidirectional freezing and freeze-drying. Whether viewed along the Z-axis and X-axis, the BT skeletons exhibit an ordered lamellar structure. As the solid content of the BT suspensions increases, the lamellar spacing of the BT skeletons gradually decreases and the lamellar thickness gradually increases. In addition, compared to the YZ plane, there are more bridges between the lamellae in the XY plane.
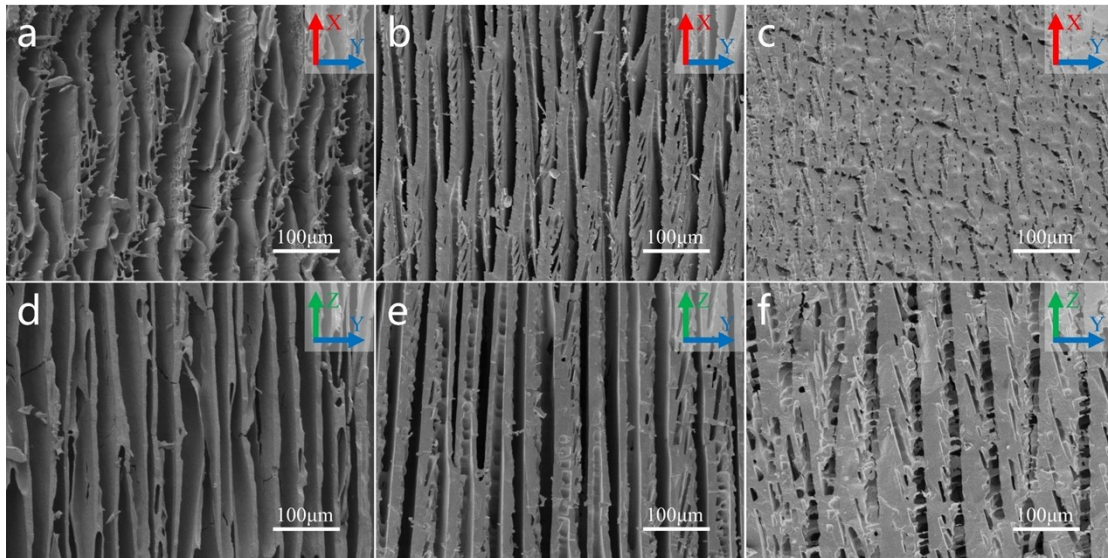
Figure S3. SEM images of the BT skeletons after sintering viewed along the (a, b, c) Z-axis and along the (d, e, f) X-axis. These skeletons were prepared from BT suspensions with (a, d) 10, (b, e) 20 and (c, f) 30 vol.% solid content.

After sintering at high temperature, the organic components in the BT skeletons were removed. Compared to the unsintered BT skeleton, the sintered BT skeletons still maintained the initial lamellar structure with no significant change in lamellar thickness. However, the lamellar spacing was slightly reduced. In addition, the BT skeleton prepared from a BT suspension with 10 vol.% solid content was slightly deformed after sintering, and the lamellae showed a slight bending.

Table S1. The specific surface area of the BT skeletons before and after calcination.

Skeleton	10 vol.%-unsintered	10 vol.%-sintered	20 vol.%-unsintered	20 vol.%-sintered	30 vol.%-unsintered	30 vol.%-sintered
Specific surface area (m^2/g)	16.330	0.046	19.151	0.055	20.210	0.061

As the solid content of the BT suspensions increased, the specific surface area of the BT skeletons gradually increased. Compared to the unsintered BT skeletons, the specific surface area of the sintered BT skeletons was significantly reduced.
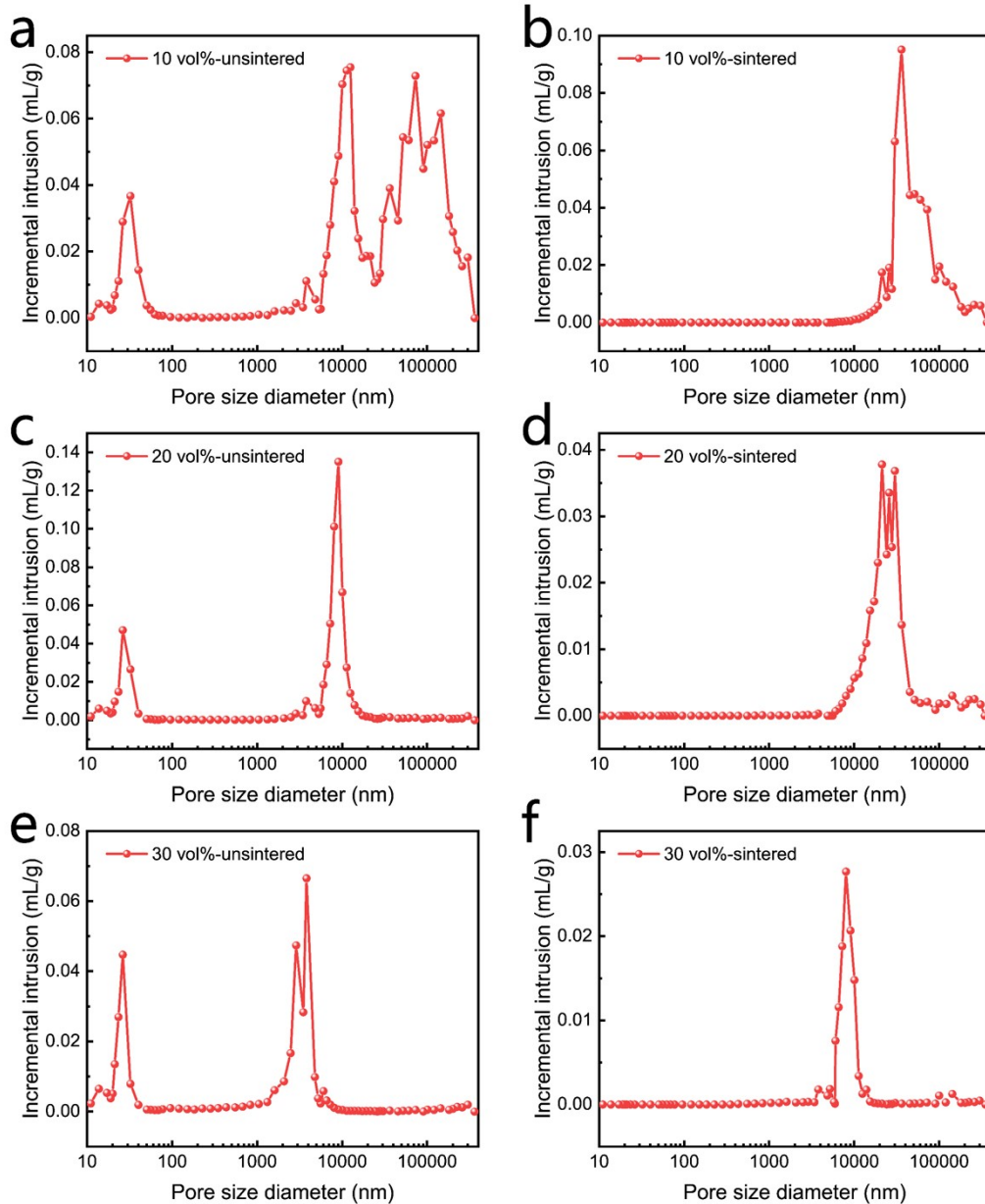
Figure S4. The pore size distribution of the BT skeletons before and after calcination.

Figure S4 shows that the BT skeletons had similar micron-sized pores before and after calcination. However, the unsintered BT skeletons also had a portion of nano-sized pores. This maybe due to the fact that the lamellae formed through bidirectional freezing were not sufficiently compact. After calcination, the BT particles were

7

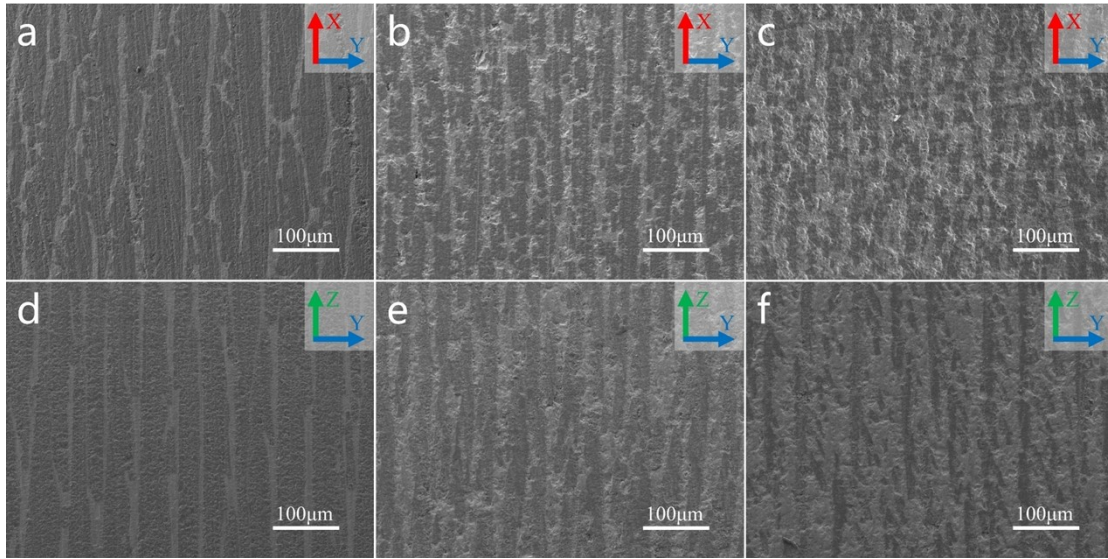interconnected and eliminated the nanopores on the lamellae.

Figure S5. SEM images of the parallel-structured BT/EP composites with different volume fractions viewed along the (a, b, c) Z-axis and along the (d, e, f) X-axis.

The parallel-structured BT/EP composites were obtained by impregnating epoxy resin into the sintered BT skeletons and curing. SEM images showed that the epoxy resin was completely impregnated into the pores of the BT skeletons with no obvious defects, and the structure of the BT skeletons was not changed. The BT and EP phases showed parallel arrangement.
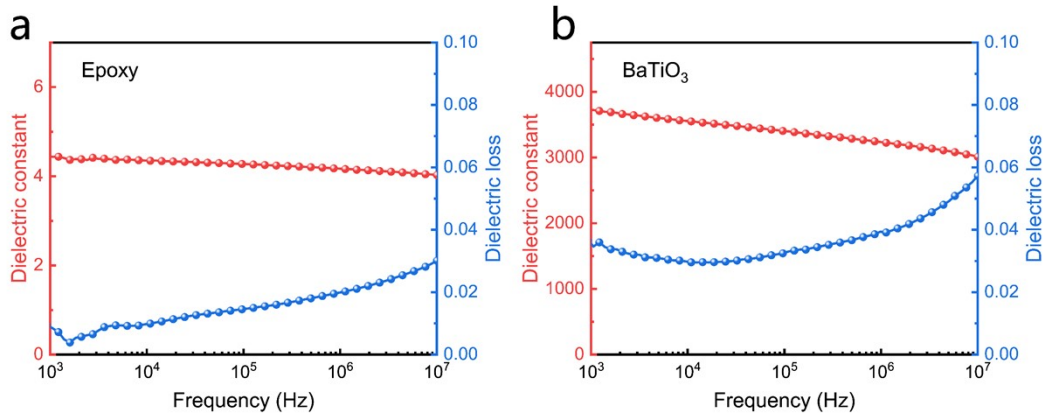
Figure S6. Frequency dependence of dielectric constants and losses of (a) pure EP and (b) BT ceramic.

The dielectric constants of both pure EP and BT ceramic decrease with increasing frequency and their dielectric constants are 4.4 and 3723 at 1 kHz, respectively. The dielectric losses of both pure EP and BT ceramic increase with increasing frequency and their dielectric losses are 0.008 and 0.034 at 1 kHz, respectively.
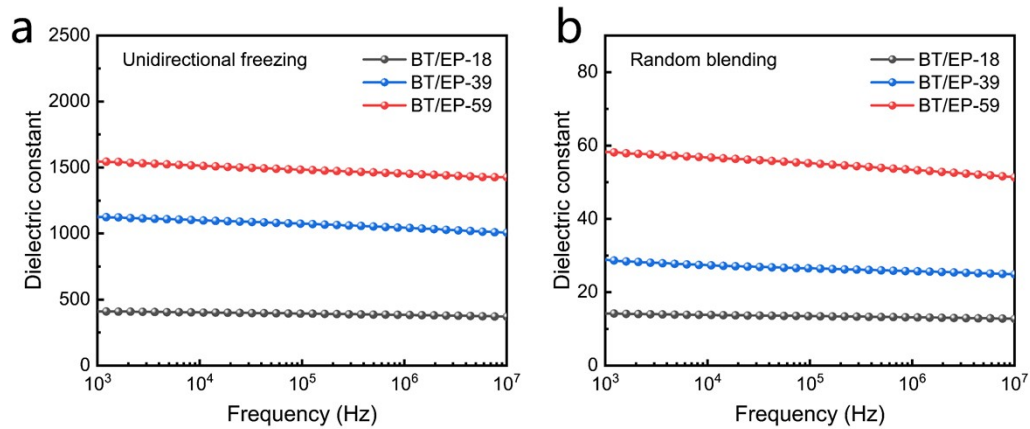
Figure S7. Frequency dependence of dielectric constants of BT/EP composites prepared by (a) unidirectional freezing and (b) random blending.

The dielectric constants of the composites prepared by unidirectional freezing and random blending increased gradually with the increase of BT volume fraction. The dielectric constants at 1 kHz of the composites prepared by unidirectional freezing are 410, 1125 and 1545, respectively. The dielectric constants at 1 kHz of the composites prepared by random blending are 14, 29 and 58, respectively.

Table S2. Comparison of the maximum polarization intensity and discharge energy density under the similar electric field conditions.

Materials	Electric field (kV/mm)	Maximum polarization intensity ($\mu C/cm^2$)	Discharge energy density (10^{-2} J/cm^3)	Reference
BT/EP	10	0.7	1.63	[1]
BT/PVDF-EP	10	0.347	1.57	[3]
BT/EP	4	11.2	11.6	[2]
BT/PVDF	3	0.143	0.16	[4]
BT/EP	10	8.8	/	[5]
BZBT/EP	10	1.6	/	[6]
BT/EP	4	24.8	13.4	This work

Table S2 listed some composites with different structures of ceramic, and compared the polarization intensity and discharge energy density under the similar electric field conditions. The parallel-structured composites exhibit higher polarization intensity and discharge energy density.
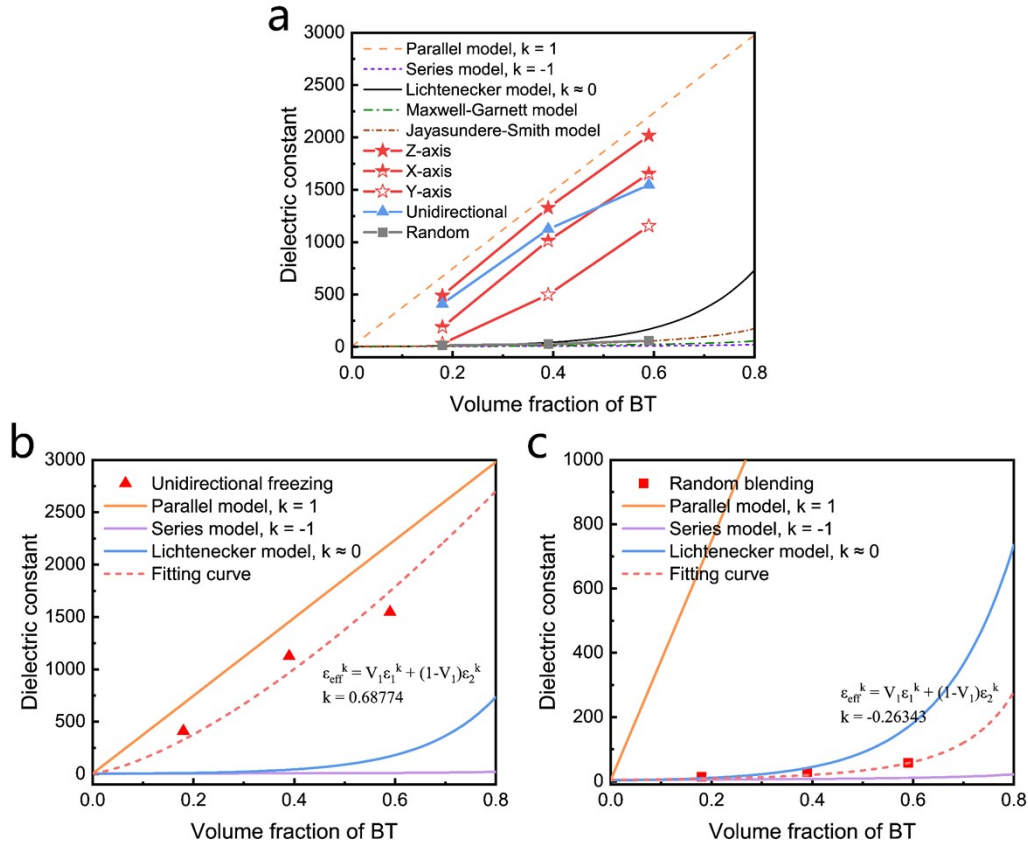
Figure S8. (a) Variation of dielectric constants of different BT/EP composites with BT volume fraction at 1kHz. Fitting curves of the BT/EP composites prepared by (b) unidirectional freezing and (c) random blending.

In order to demonstrate that the parallel-structured composites can more effectively utilize the intrinsic high dielectric properties of the ceramic fillers and greatly improve the dielectric constants of the composites, five commonly used theoretical models (eqn (S1) - (S5)) are employed here to compare with the experimental results of the parallel-structured composites and the two comparison composites. Based on the fitting curves of the dielectric constant, the k-values of the composites prepared by unidirectional freezing is 0.69. However, the k-value of the composites prepared by random blending is only -0.26.
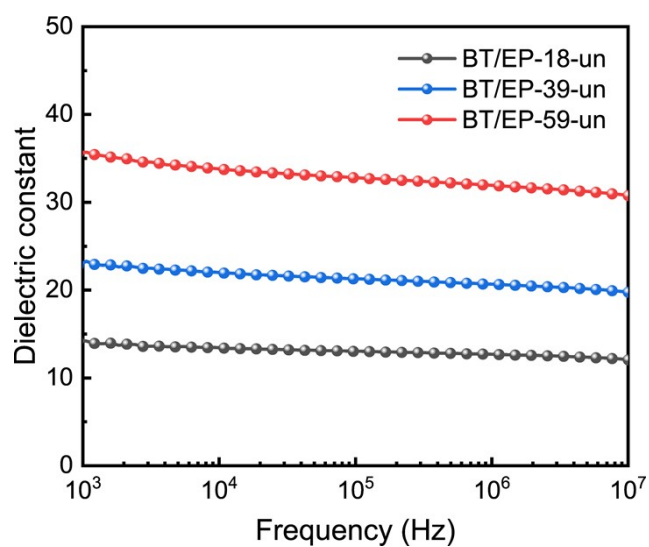
Figure S9. Frequency dependence of dielectric constants of the BT/EP composites with unsintered BT skeletons.

The dielectric constants of the BT/EP composites with unsintered BT skeletons increased gradually with the increase of BT volume fraction. The dielectric constants at 1 kHz of the composites are 14, 23 and 36, respectively.
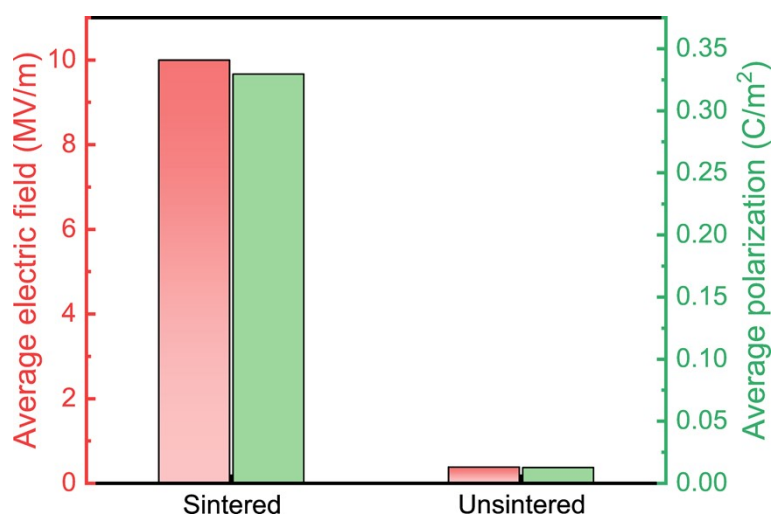
Figure S10. Average local electric field intensity and average polarization intensity of the sintered and unsintered BT skeletons.

The average local electric field intensity and average polarization intensity of the sintered BT skeleton are 10 MV/m and 0.330 C/m^2, respectively. In contrast, the average local electric field intensity and average polarization intensity of the unsintered BT skeleton are only 0.39 MV/m and 0.013 C/m^2, respectively.
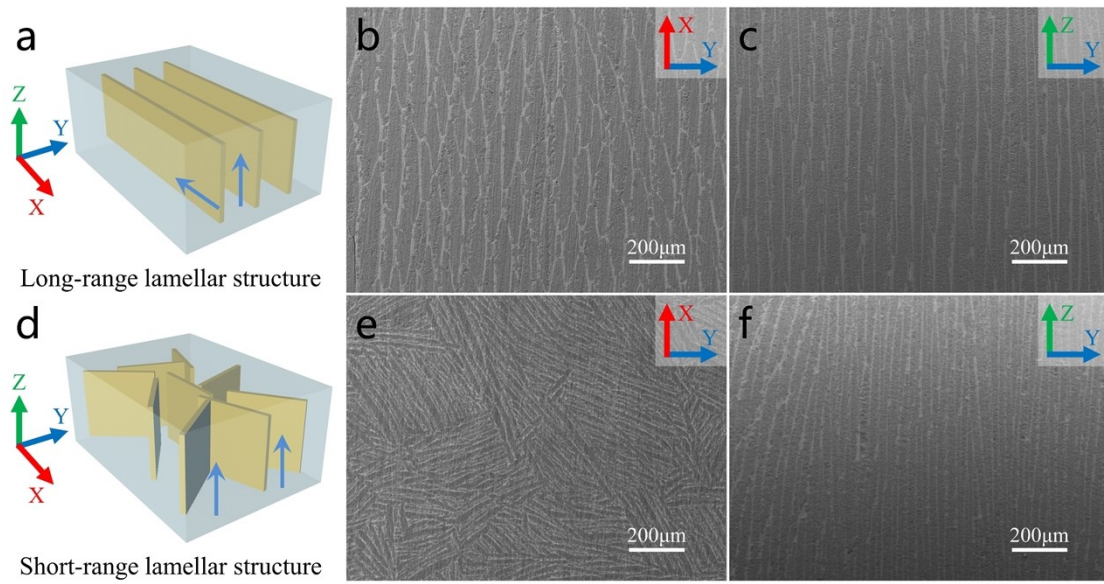
Figure S11. Models and SEM images of (a, b, c) the parallel-structured composites and (d, e, f) composites prepared by unidirectional freezing.

In addition, the structures of the parallel-structured composites and the composites prepared by unidirectional freezing are compared, and the reasonable explanation is given for the lower dielectric constants of the composites prepared by unidirectional freezing than those of the parallel-structured composites when the electric field is along the Z-axis: i) The composites prepared by unidirectional freezing are less regular and ordered than the parallel-structured composites, and the BT lamellae are not completely parallel to the Z-axis direction; ii) The composites prepared by unidirectional freezing are short-range lamellar structure which have more interfaces between BT and EP. These two reasons lead to more interfacial polarization in the composites prepared by unidirectional freezing, which suppresses the contribution of BT.

References

1. S. Luo, Y. Shen, S. Yu, Y. Wan, W.-H. Liao, R. Sun and C.-P. Wong, *Energy Environ. Sci.*, 2017, **10**, 137-144.

2. R. Guo, J. I. Roscow, C. R. Bowen, H. Luo, Y. Huang, Y. Ma, K. Zhou and D. Zhang, *J. Mater. Chem. A*, 2020, **8**, 3135-3144.

3. Z. Zhang, S. Luo, S. Yu, Z. Guan, R. Sun and C.-P. Wong, *Mater. Des.*, 2018, **142**, 106-113.

4. X. Bi, L. Yang, Z. Wang, Y. Zhan, S. Wang, C. Zhang, Y. Li, Y. Miao and J. Zha, *Materials*, 2021, **14**.

5. M. Cao, X. J. Yan, L. Li, S. Y. Wu and X. M. Chen, *ACS Appl. Mater. Interfaces*, 2022, **14**, 7039-7051.

6. T. Tang, W. Yang, Z. Shen, J. Wang, M. Guo, Y. Xiao, W. Ren, J. Ma, R. Yu, C. W. Nan and Y. Shen, *Adv. Mater.*, 2023, **35**, e2209958.